**Preprint Title** Crossover between superconducting and boron-carbon phases in heavily boron-doped diamond homoepitaxial layers

**Authors** Ekaterina A. Arkhipova, Denis A. Savinov, Mikhail N. Drozdov, Pavel A. Yunin, Stanislav A. Kraev, Mikhail A. Lobaev, Dmitry B. Radishev, Sergey A. Bogdanov, Alexey M. Gorbachev, Anatoly L. Vikharev, Anna V. Gordeeva, Victoria Y. Safonova, Leonid S. Revin and Andrey L. Pankratov

**Publication Date** 07 Sept. 2026

**Article Type** Full Research Paper

**ORCID® iDs** Denis A. Savinov - https://orcid.org/0000-0002-7489-6087; Mikhail A. Lobaev - https://orcid.org/0000-0002-7261-6766; Dmitry B. Radishev - https://orcid.org/0000-0002-8416-1738; Leonid S. Revin - https://orcid.org/0000-0003-1645-4122; Andrey L. Pankratov - https://orcid.org/0000-0003-2661-2745

# Crossover between superconducting and boron-carbon phases in heavily boron-doped diamond homoepitaxial layers

E.A. Arkhipova*[1], D.A. Savinov[1], M.N. Drozdov[1], P.A. Yunin[1], S.A. Kraev[1], M.A. Lobaev[2], D.B. Radishev[2], S.A. Bogdanov[2], A.M. Gorbachev[2], A.L. Vikharev[2], A.V. Gordeeva[3], V.Yu. Safonova[3], L.S. Revin[1,3], A.L. Pankratov[1,3]

Address: [1]The Institute for Physics of Microstructures of the Russian Academy of Sciences, 603950, Russia, Nizhny Novgorod, Academicheskaya St.7,[2]Federal Research Center A.V. Gaponov-Grekhov Institute of Applied Physics of the Russian Academy of Sciences, 603951, Russia, Nizhny Novgorod, 46 UlyanovStr, [3]Nizhny Novgorod State Technical University n.a. R.E. Alekseev, 603155, Russia, Nizhny Novgorod, Minin Street, 24

Email: Ekaterina Alexandrovna Arkhipova - suroveginaka@ipmras.ru

* Corresponding author

## Abstract

Homoepitaxial diamond films heavily doped with boron, grown by CVD on single-crystal type IIa diamond substrates are investigated. Quantitative analysis of the nominal, structural, and active concentrations of boron atoms in the grown layers was made using secondary ion mass spectrometry, X-ray diffractometry, and van der Pauw method, respectively. Nominal concentrations ranged from $8.2 \cdot 10^{20}$ $cm^{-3}$ to

$2 \cdot 10^{22}$ $cm^{-3}$. Electrophysical measurements revealed metallic conductivity in the epitaxial layers, and a superconducting transition was observed. The dependence of the superconducting critical temperature on the boron doping level was studied. At nominal concentrations of $10^{22}$ $cm^{-3}$ and higher, diamond lost its perfection, transitioning to a graphite-containing phase that lacks the superconducting transition. Thus, this study examined the crossover from the superconducting phase to the boron-carbon phase with a gradual increase in the nominal boron concentration. The critical boron doping level was determined for diamond to exhibit superconductivity while maintaining its crystalline perfection, which is an important parameter for the formation of heavily doped diamond layers with a superconducting transition.

## Keywords

heavily boron-doped homoepitaxial layers of CVD diamond, superconducting transition, superconducting critical temperature, boron carbide, secondary ion mass spectrometry, X-ray diffractometry, van der Pauw method, Raman spectroscopy, electrophysical measurements

## Introduction

Diamond possesses unique physical properties: exceptional hardness, high thermal conductivity, it is an ultra-wide band gap (UWBG) semiconductor, what makes this material promising for use in modern technologies [1, 2]. Single-crystal diamond doped with boron is of particular interest for applications. Boron is relatively easily incorporated into the diamond crystal lattice due to the closeness of its covalent radius (82 pm) to that of carbon (77 pm). This allows diamond to be doped to relatively high concentrations, producing a semiconductor material with low resistivity

[3]. Natural diamonds doped with boron are quite rare. Furthermore, the maximum boron concentration found in natural crystals is relatively low, approximately $10^{17}$ $cm^{-3}$, limiting their potential applications. To produce synthetic diamond heavily doped with boron, the high-pressure high-temperature (HPHT) and chemical vapor deposition (CVD) methods are used. HPHT allows the creation of thick layers doped with boron with a concentration of $10^{19}$–$10^{20}$ $cm^{-3}$ [4]. CVD allows the production of diamonds with a dopant concentration 1–2 orders of magnitude higher than HPHT. Most studies of the electrical properties of boron-doped diamonds are currently conducted on layers obtained by CVD. However, with heavy boron doping, the structural perfection of the diamond is compromised due to the presence of mechanical stresses and dislocations. A detailed study of the structural features and electrical properties of boron-doped diamond is necessary for the subsequent use of this material in the creation of active and passive electronic devices based on it.

Superconductivity is observed in diamond heavily doped with boron. This phenomenon was first found in heavily boron-doped polycrystalline diamond synthesized in a high-pressure cell [5]. Later, superconductivity was observed in boron-doped poly- and single-crystal CVD diamond films with boron concentrations above $10^{20}$ $cm^{-3}$ [6-10]. The structure of impurity bands and their influence on the critical transition temperature $T_c$ were considered in [11]. Relaxation of the resistive superconducting state in boron-doped diamond films was studied in [12].

The superconducting transition temperature $T_c$ strongly depends on the boron impurity concentration in diamond. As a rule, superconductivity is observed at boron concentrations greater than $5 \cdot 10^{20}$ $cm^{-3}$, when the transition to metallic conductivity occurs in diamond. According to [6] and [9], an increase in the critical transition temperature $T_c$ with an increase in the boron concentration occurs up to a value of $10^{22}$ $cm^{-3}$ and even higher. However, at such high concentrations, saturation of boron

incorporation can occur with a subsequent transition of diamond to a binary compound of boron with carbon (boron carbide). In [13], the superconducting transition was observed only up to a concentration of $3 \cdot 10^{21}$ $cm^{-3}$. The critical level of doping of CVD diamond with boron atoms, at which diamond retains its perfection, is a necessary parameter for the creation of heavily doped superconducting diamond layers and the observation of the superconducting transition in such structures. It should be noted that the boron concentration range from $5 \cdot 10^{20}$ $cm^{-3}$ to $10^{22}$ $cm^{-3}$ has not been sufficiently explored in the literature for the controlled production of high-crystalline homoepitaxial layers and the observation of the superconducting transition. Most studies have focused on achieving the maximum $T_c$ value at the expense of the quality of the resulting heavily doped diamond layers.

In this paper, we used various experimental methods to study changes in the active concentration of boron atoms in epitaxial layers with a gradual increase in the doping level (nominal concentration). We also examined the structural and superconducting properties of the layers, analyzed the transition from the superconducting phase to the boron-carbon phase, and determined the critical nominal concentration at which diamond maintains its perfection. The primary focus was on producing CVD layers with high crystalline perfection and an atomically smooth surface for future applications in both semiconductor electronics and the creation of superconducting elements.

# Results

The boron atom concentration profiles measured by SIMS in heavily doped layers grown on HPHT substrates S1, S2, and S3 with a (001) crystal orientation are shown in Figure 1. These data determine the average nominal (total) concentration of boron

atoms in the CVD diamond layers. As can be seen from the figure, the CVD diamond layer grown on substrate S3 has two sublayers of approximately the same thickness (500 nm) but with different boron concentrations. The highest boron concentration, approximately $10^{22}$ $cm^{-3}$, was achieved in the surface sublayer.

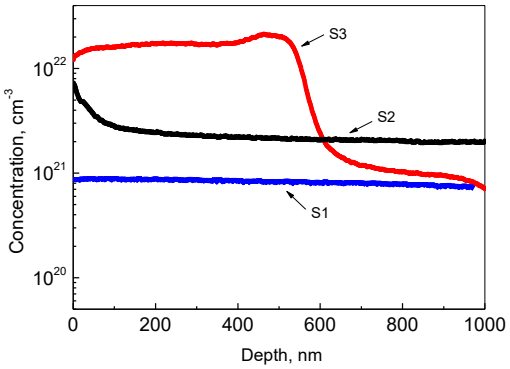


**Figure 1:** Profiles of boron atom concentrations in layers grown on HPHT substrates S1, S2 and S3 obtained by SIMS measurements.

Figure 2 shows the XRD-measured rocking curves for the (004) reflection for the same heavily boron-doped homoepitaxial layers. For each sample, two characteristic peaks were observed: a peak associated with the HPHT substrate and a peak associated with the deformed heavily boron-doped layer with an increased lattice size. The boron concentration in the layer was estimated from the rocking curves shown in Figure 3 based on the angular distance between the peaks of the layer and the substrate in the approximation of boron substitution for carbon. The concentration was determined using a growth model of an elastically stressed pseudomorphictetragonally deformed doped layer [14, 15].

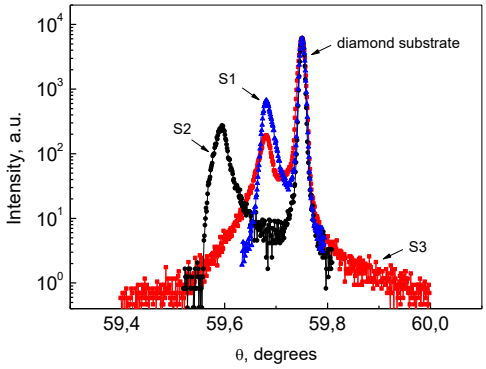


**Figure 2:** Rocking curves of the (004) reflection for homoepitaxial heavily boron-doped layers grown on HPHT substrates S1, S2, S3.

Electrophysical measurements allowed us to compare the change in the active boron concentration with increasing doping level. Table 1 presents the nominal/structural/active boron atom concentrations determined by SIMS, XRD, and van der Pauw measurements, respectively. It is noteworthy that the resulting CVD diamond films exhibited high conductivity. The layer on the S2 substrate had the lowest resistivity at room temperature, equal to $\rho = 10^{-3}\,\Omega\cdot cm$.

**Table 1:** Nominal/structural/active concentration of boron atoms, specific resistance ρ and superconducting critical temperature $T_c$ in layers grown on HPHT substrates S1, S2, S3.

| Sample | $N_B$, $cm^{-3}$ SIMS | $N_B$, $cm^{-3}$ XRD | p, $cm^{-3}$ Van der Pauw | ρ, Ω·cm | $T_c$, K |
|---|---|---|---|---|---|
| S1 | $8.3\cdot10^{20}$ | $6.7\cdot10^{20}$ | $6.7\cdot10^{20}$ | $3.8\cdot10^{-3}$ | - |
| S2 | $2\cdot10^{21}$ | $1.5\cdot10^{21}$ | $1.8\cdot10^{21}$ | $10^{-3}$ | 1.6 |
| S3 | $10^{21}$-$2\cdot10^{22}$ | $7\cdot10^{20}$ | $9\cdot10^{20}$ | $2.9\cdot10^{-3}$ | 0.035 |

Figure 3 shows the Raman spectra for samples S1, S2, and S3. Heavily doped diamond layers exhibit features (peaks) in the Raman scattering spectrum that are observed in the wavelength range of 400–1300 $cm^{-1}$ [16, 17]. They are associated with the Fano effect in Raman scattering – the interaction of a discrete phonon mode with a continuum of electronic excitations (free charge carriers). Following [16, 17], to approximate the Raman scattering shape, we used the Breit-Wigner-Fano (BWF) function, which characterizes Raman modes by accounting for asymmetric line shapes caused by quantum interference. The spectrum was presented as a sum of the following components: 1 - the peak located at 500 $cm^{-1}$ characteristic of heavily boron-doped diamond and 2 - an additional peak located at ca. 1100 $cm^{-1}$, 3 - the peak located at 1200 $cm^{-1}$ attributed to a maximum of the phonon density of states, 4 - diamond line located at ca. 1332 $cm^{-1}$ and graphite G-band around 1560 $cm^{-1}$ (observed only for sample S3) [16].

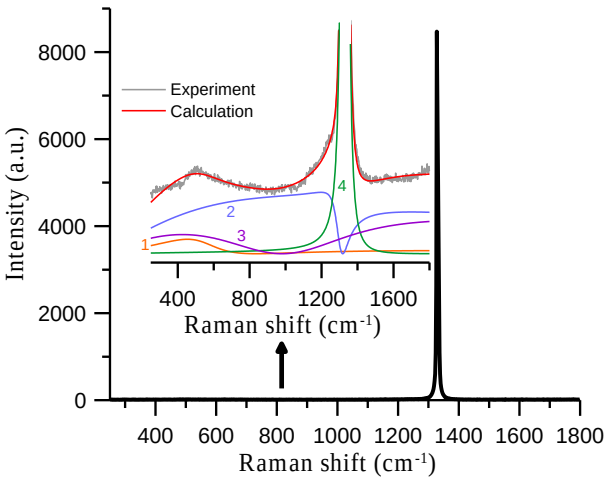


(a)

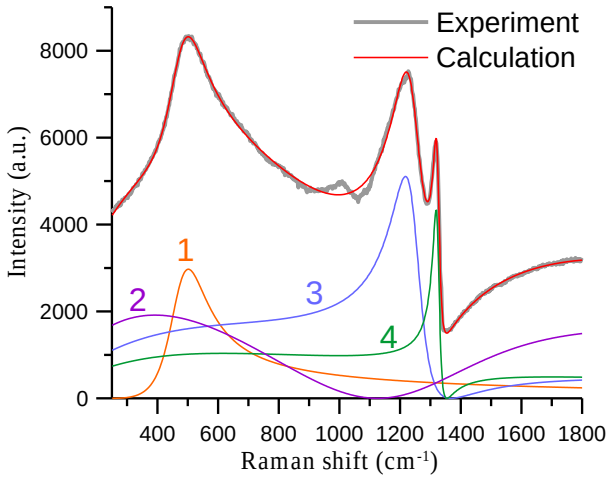


(b)

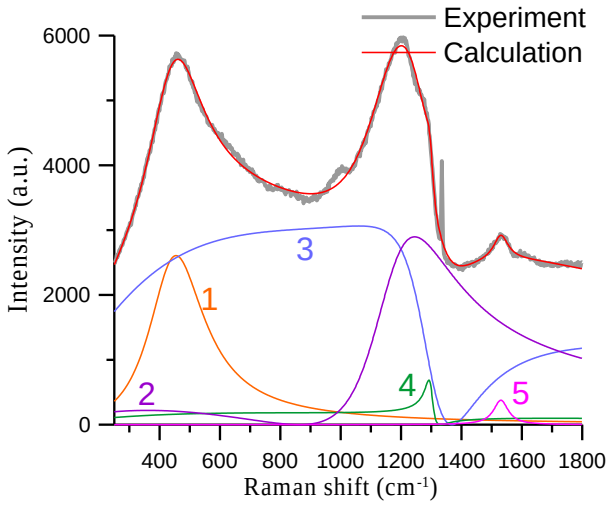


(c)

Figure 3: Raman scattering spectrum for samples S1(a), S2(b), S3(c). The Breit-Wigner-Fano formula with components at wavelengths of 1 – 500 $cm^{-1}$, 2 – 1100 $cm^{-1}$, 3 – 1200 $cm^{-1}$, 4 – 1332 $cm^{-1}$, 5 – 1560 $cm^{-1}$ (observed only for sample S3) was used to approximate the spectrum.

At low doping levels (S1), no asymmetry of the diamond peak was observed, and the boron-related peaks were much smaller than the diamond peak (Fig. 3a). At higher doping levels (S2), strong asymmetry of the diamond peak was observed, and the boron-related terms coincided with its amplitude (Fig. 3b). Minimal resistivity of the obtained layers was also observed. With a further increase in boron concentration

(S3), the diamond-related peak practically disappeared from the Raman spectrum, and a graphite-related peak appeared (see Fig. 3c, magenta curve).

After growth, the surface morphology of the grown layers was also studied using a ZygoNewView 7300 white light interferometer over an area of 0.22×0.22 mm. The root-mean-square surface roughness for samples S1 and S2 increased slightly after growth and ranged from 0.3 to 0.5 nm. Thus, for samples S1 and S2, diamond crystal growth was achieved through sequential filling of atomic planes (step-flow growth) [18]. For sample S3, the root-mean-square roughness increased to 8 nm, indicating deterioration in the quality of epitaxial growth.

The superconducting properties of samples S1, S2, and S3 were studied in a dry dilution refrigerator. Figure 4 shows a graph of the superconducting transition *R(T)* of diamond in sample S3. The measuring current was 1 μA. The critical temperature $T_c$ was about 35 mK, the transition width was approximately 1 mK.

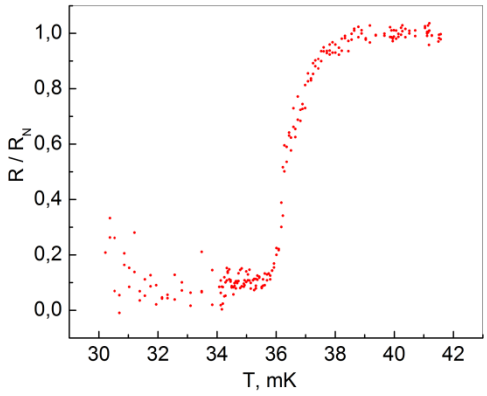


Figure 4: Temperature dependence of resistance *R(T)* for diamond sample S3.

Further studies included measurements of the I–V characteristics of the diamond layers. Figure 5 shows the temperature dependence of the critical current, obtained from the I–V characteristics for sample S2 at different temperatures (inset). The

occurrence of a critical current at approximately 1.6 K indicates the sample's transition to the superconducting state at this temperature.

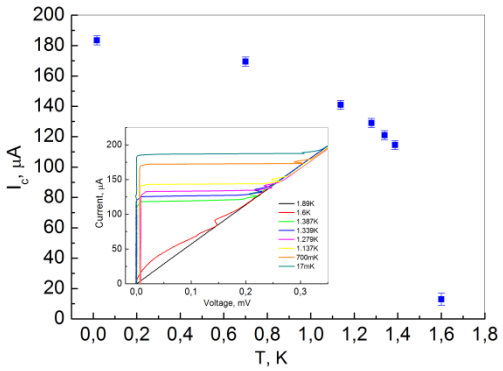


Figure 5: Temperature dependence of the critical current and I–V characteristics for the epitaxial layer on substrate S2 at various temperatures.

# Discussion

By comparing the average boron concentration in the layers as measured by SIMS and XRD data (see Table 1), one can understand how boron atoms are incorporated into the diamond crystal lattice. SIMS measurements indicate the total boron concentration (including boron incorporated into interstitial sites and not contributing to conductivity) — the nominal concentration. XRD measurements provide an estimate of the structural boron impurity (boron atoms substituting for carbon atoms in the lattice) — the structural concentration. Good agreement between the SIMS and XRD results for samples S1 and S2 indicates that boron atoms are incorporated into the diamond crystal lattice sites without significantly deforming it. Electrical measurements using the Hall effect method in van der Pauw geometry allowed us to estimate the active concentration of boron atoms — the hole concentration. For samples S1 and S2, the nominal, structural, and active concentrations are similar. For sample S3, a significant difference between the nominal and structural

concentrations of boron atoms in the near-surface layer of approximately 500 nm is observed, which may be due to the formation of a boron-carbon phase in the layer. At a nominal concentration of boron atoms of approximately $10^{22}$ $cm^{-3}$, diamond loses its perfection, and the structural concentration becomes significantly lower. This is also confirmed by the results of Raman spectroscopy: a peak corresponding to the appearance of a graphite-like $sp^2$ phase appears in the Raman spectra (see Fig. 3c). Moreover, for the sublayer immediately above the substrate, also 500 nm thick (see Fig. 1 S3 at a depth of 500–1000 nm), the SIMS and XRD measurement data agree well. Namely in this sublayer the superconducting transition with a critical temperature of approximately 35 mK occurs. As follows from the correspondence of the peaks in Fig. 2 for samples S3 and S1, as well as from the SIMS measurement profiles in Fig. 1, superconductivity in these layers occurs at a nominal boron concentration of approximately $10^{21}$ $cm^{-3}$. We also note that the correspondence between the active and structural concentrations indicates the metallic nature of conductivity in the studied samples, which is a necessary condition for observing the superconducting transition.

It is noteworthy that a critical transition temperature $T_c$ of approximately 35 mK and a transition width of approximately 1 mK were detected in the epitaxial layer of sample S3. Such a low $T_c$ and the sharpness of the observed transition are of interest for the creation of low-temperature sensors for particle physics and microwave signal detection – microcalorimeters and bolometers, the so-called TES (Transition Edge Sensor) detectors [19, 20] based on homoepitaxial heavily doped diamond films. Superconducting TES detectors are rather sensitive sensors, suitable for for detecring single photons, including X-rays, dark matter particles, and neutrinos. The energy resolution of TES is determined by the operating range of critical temperatures $T_c$, and optimal values are 15–100 mK. Furthermore, the use of a

substrate with a high Debye temperature $T_D$ (diamond has a $T_D$ of 2200 K) in TES detectors enables the creation of high-quality thermal insulators, minimizing parasitic heat capacity and increasing detector sensitivity, while the high thermal conductivity of diamond effectively prevents overheating of the working region. These factors combined allow such films to be considered as an alternative to traditional materials [21, 22, 23] for highly sensitive TES microcalorimeters.

# Conclusion

In this study, several epitaxial layers were grown on diamond HPHT substrates with a (001) crystal orientation and boron doping levels ranging from $8.3 \cdot 10^{20}$ $cm^{-3}$ to $2 \cdot 10^{22}$ $cm^{-3}$. Homoepitaxial diamond films with a nominal concentration of $(1–3) \cdot 10^{21}$ $cm^{-3}$ exhibited high crystalline perfection and a sharp doping profile, as well as high conductivity. The lowest resistivity at room temperature was obtained for the layer in sample S2 and amounted to $\rho = 10^{-3}$ Ω·cm. Good agreement between the nominal and structural concentrations of boron atoms for this layer indicates that the boron atoms were embedded in the diamond crystal lattice sites without deforming it or forming boron-carbon and/or graphite-like phases. It was found that layers with a boron atom concentration of ~ $2 \cdot 10^{21}$ $cm^{-3}$ had a superconducting transition with a maximum possible temperature $T_c$ ~ 1.6 K. In the work, a crossover from the superconducting phase to the boron-carbon phase was observed with a gradual increase in the nominal boron concentration, which was accompanied by the appearance of doping inhomogeneity, a decrease in the structural concentration of boron and an increase in specific resistance, as well as the appearance in the Raman scattering spectrum of a peak corresponding to a graphite-like phase.

# Methods

Homoepitaxial layers heavily doped with boron with a thickness of several microns were grown on type IIa HPHT diamond substrates measuring 3.5×3.5×0.5 $mm^3$ with a (001) crystal orientation. The substrates used for the growth process had a surface roughness of 0.2 nm, measured using a ZygoNewView 7300 white light interferometer on an area of 0.22×0.22 mm. Layers growth was performed in a CVD reactor developed at the Institute of Applied Physics of the Russian Academy of Sciences, in which a microwave discharge plasma in a gas mixture of hydrogen and methane with the addition of diborane $H_2$-$CH_4$-$B_2H_6$ was maintained using magnetron radiation at a frequency of 2.45 GHz [24]. A series of experiments on diamond doping with boron were conducted, with increasing of the boron content in the working gas mixture. To demonstrate the characteristic features of doping, samples S1, S2, S3 with different levels of boron concentration were selected.

The study of homoepitaxial heavily doped CVD diamond layers was performed by X-ray diffractometry (XRD) on a Bruker D8 Discover diffractometer in a high-resolution configuration with a 4xGe (220) quadruple-reflection monochromator. Rocking curves for the (004) diamond reflection were recorded, revealing a peak from the diamond substrate and a separate peak corresponding to the heavily boron-doped CVD diamond layer. Empirical relationships from [14, 15] were used to estimate the structural concentration of boron in the doped layers.

The study also utilized secondary ion mass spectrometry (SIMS) method, which allowed the boron atom distribution profile to be determined across the layers' depths. The nominal boron concentration in the layers was determined using this method. SIMS measurements were performed on a TOF.SIMS-5 setup with separate

ion beam functions (sputtering and probing). Sputtering was performed with 1 keV $Cs^+$ ions, and probing with 25 keV $Bi^+$ or $Bi^{3+}$ ions.

The active concentration of boron atoms (hole concentration) and the resistivity of the diamond layer were estimated using Hall-effect measurements in van der Pauw geometry.

Raman spectroscopy was used to study the degree of crystalline perfection and the presence of non-diamond carbon phases in highly boron-doped diamond layers. This technique allows the detection of non-diamond forms of carbon (in particular, the graphite-like phase) by detecting the corresponding scattering lines in the spectrum. Measurements were performed on a RenishawinVia Reflex confocal Raman microscope with a laser operating at a wavelength of 514 nm.

To study the superconducting properties of a heavily boron-doped homoepitaxial CVD diamond layer, the temperature dependences of the layer resistance and its I-V characteristics were measured. The studies were conducted using a four-probe setup in a closed-loop cryostat at temperatures up to 10–15 mK. Figure 6 shows a photograph of a sample with test cells formed on the surface of the epitaxial layer, the contact pads measured 100×100 $\mu m^2$. Contact to these pads was made using an ultrasonic bonding machine with an aluminum wire with a diameter of 30 μm. Ohmic contacts to the diamond were formed using electron-beam evaporation and consisted of Ti/Mo/Au layers with thicknesses of 20/30/100 nm.

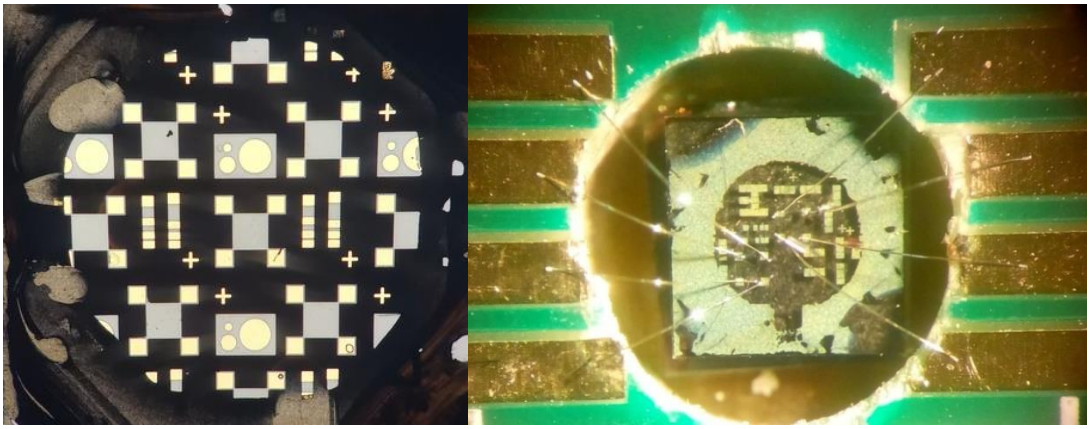

Figure 6: Photograph of a diamond sample from the side of the CVD layer with deposited contacts. (left) – test structures on the diamond, (right) – the test sample welded onto the PCB board.

## Acknowledgements

This work utilized equipment from the IAP RAS Center for Collective Use "Physics and Technology of Micro- and Nanostructures".

## Funding

The synthesis of diamond layers was carried out within the frame of the Institute of Applied Physics of the Russian Academy of Sciences Project FFUF-2024-0032.

The electrophysical measurements were carried out within the framework of the IAP RAS state assignment, FFUF-2025-0006.

Measurements of superconducting properties of diamond structures were carried out within the framework of the IAP RAS state assignment, FFUF-2024-0024.

## References

1. Zulkharnay,R.; May,P.W.;*Functional Diamond*,**2024**, *4*, 2410160.

2. May, P.W.;Zulkharnay, R;*Phil. Trans. R. Soc.*, **2025**,*A 383*: 20230382.

3. Ohmagari, S.;*Functional Diamond*,**2023,***3*, 2259941.

4. Bormashov,V.S.;Tarelkin,S.A.;Buga, S.G.; et al.*Diam. Relat. Mater.*,**2013**,*35*, 19-23.

5. Ekimov, E.A.;Sidorov, V.A.; Bauer, E.D.; et al. *Nature*,**2004**,*428*, 542–545.

6. Takano, Y.; Nagao, M.;Sakaguchi, I.; et al. *Appl. Phys. Lett.*,**2004**,*85*, 2851-2853.

7. Bustarret, E.;Kačmarčik, J.;Marcenat, C.; et al. *Phys Rev Lett.,***2004***, 93,*237005

8. Takano, Y.;*J. Phys.: Condens. Matter*, **2009**,*21*, 253201.

9. Kawano, A.; Ishiwata, H.; Iriyama, S.; et al. *Phys. Rev*. B, **2010**, *82*, 085318.

10. Kitagoh, S.; Okada, R.; Kawano, A.; et al. *Physica C: Superconductivity and its Applications*, **2010**, *470*, S610–S612.

11. Kumara, D.;Chandran, M.;Shukla,D.K.; et al. *Physica C: Superconductivity and its Applications*, **2018**, *555*, 28-34.

12. Kardakova, A.;Shishkin,A.; Semenov,A.; et al. *Phys. Rev. B*, **2016**, *93*, 064506.

13. Bousquet J.; Klein T.; et al. *Phys. Rev. B*, **2017***, 95 (16),* pp.161301.

14. Brunet,F.;Germi,P.;Pernet,M.; et al.*J. Appl. Phys.*,**1998**,*83*, 181-186.

15. Wojewoda,T.;Achatz,P.;Ortéga,L.; et al.*Diam. Relat. Mater.*,**2008**,*17*, 1302-1306.

16. Mortet, V.; Gregora, I.; Taylor, A.; et al.*Carbon*, **2020**,*168*, 319-327.

17. Dwivedi, J.; Islam, S.; Morris, J.; et al.*PNAS*,**2026**,*123*, e2607730123.

18. Ogura, M.; Kato, H., Makino, T., *J. Cryst. Growth*, **2011**, *317*, 60-63.

19. Irwin, K.D.; Hilton, G.C.;*Cryogenic Particle Detection. Topics in Applied Physics,* **2005**, *99*, 63–150.

20. Safonova,V.Yu.;Gordeeva, A.V.;Blagodatkin, A.V.; et al.*Beilstein Journal Nanotechnology*, **2024**,*15*, 1353–1361.

21. Hennings-Yeomans, R.; Chang, C. L.; Ding, J; et al. J. App. Phys.,**2020**, *128*, 154501.

22. Drozdov, M.N.;Daniltsev, V.M.;Arkhipova, E.A.; et al.*Physics of the Solid State*, **2024**, *66*, 1039–1043.

23. Gordeeva A.V., Safonova V.Yu., Blagodatkin A.V., Yablokov A.A., Pankratov A.L. Hf-based transition-edge sensor with a critical temperature below 100 mK // Supercond. Sci. Technol. – 2026. – Vol. 39. – No. 7. – P. 075014.

24. Vikharev, A.L.; Gorbachev, A.M.;LobaevM.A.; et al.*Phys. Status Solidi RRL*, **2016**, *10*, 324-327.